IEEE Access
Multidisciplinary | Rapid Review | Open Access Journal

Received October 19, 2018, accepted November 20, 2018, date of publication November 27, 2018,
date of current version December 27, 2018.

Digital Object Identifier 10.1109/ACCESS.2018.2883503

Study of Maximum Power Delivery to Movable Device in Omnidirectional Wireless Power Transfer System

MEI SU[1,2], ZIXI LIU[1,2], QI ZHU[1,2], (Student Member, IEEE), AND AIGUO PATRICK HU[3], (Senior Member, IEEE)

[1]School of Information Science and Engineering, Central South University, Changsha 410083, China
[2]Hunan Provincial Key Laboratory of Power Electronics Equipment and Grid, Changsha 410083, China
[3]Department of Electrical and Computer Engineering, The University of Auckland, Auckland 1023, New Zealand

Corresponding author: Qi Zhu (csu_zhuqi@163.com)

The early stage researcher is supported by the National Natural Science Foundation of China under Grant 51677195 and Grant 61622311. The funding for experimental facilities is supported by the scholarship from the China Scholarship Council under Grant CSC 201706370068. And the charge for publication is supported by the Project of Innovation-driven Plan in Central South University under Grant 2019CX0003.

ABSTRACT More mobile devices are now being charged wirelessly due to the convenience, ease of use, and competitive power efficiency of wireless power transfer. However, traditional wireless power transfer systems are not applicable if the mobile devices need to be charged while moving. This paper focused on an omnidirectional wireless power transfer system, which has the potential to transfer power to a movable device. And two different maximum power delivery methods are proposed for applications with intermittently and frequently moving devices. By analyzing the relationship between the input power of the system and the load power, the communication link between the transmitter and the receiver is eliminated. Both methods satisfied the need of dynamic charging for the movable device. The parameter identification method is more suitable for the device which moves intermittently, while the gradient descent method aims at charging the frequently moving devices. Based on the circuit model of the omnidirectional WPT system, the two methods have been mathematically modeled, and the corresponding algorithms for maximum power transfer are proposed. Then, a prototype is implemented to validate the proposed methods. Experimental results have shown that both the methods can be used to achieve maximum output power during the movement of power pickups. At steady-state, a maximum power of 37.08W at 70.39% efficiency has been achieved using the parameter identification method; while 36.48W at 69.90% has been achieved using the gradient descent method.

INDEX TERMS Gradient descent, maximum power delivery, movable device, omnidirectional wireless power transfer system, parameter identification.

I. INTRODUCTION

Wireless power transfer (WPT) becomes an emerging solution for power delivery to electric devices due to its convenience and safety, especially in smart mobile, medical implants, home appliances, industrial equipment and electric vehicles [1]–[7].

In the early stage, the delivered power level and overall efficiency of the WPT system are the most concerned by the researchers and engineers. Lots of methods have been studied by the scholars to improve the performance of inductive power transfer (IPT) or capacitive power transfer (CPT) system, such as megahertz operation frequency [8], compensation network improvement [9], maintaining system resonance [10] and refactoring coil structure [11].

With the maturity of the WPT technology, the range of wireless power transfer and the space freedom of the power pick-up have attracted more attention. For a planar WPT system, Lei Zhao and Udaya K. Madawala et al proposed a novel series-hybrid topology to provide a constant power transfer over a wide range of spatial displacements [12], [13]. However, the planar WPT systems are hard to deal with the problems of the angular rotation and positional shift in a relatively wide range. If a wirelessly charged device with a demand for higher mobility is arbitrarily located in a confined space, those WPT techniques are not applicable.

A high-dimensional WPT system which can transfer power to an arbitrary location within a defined space would be beneficial. Up to now, some IPT systems have applied the

technology of magnetic field shaping, which allows directional energy transfer [14]–[23]. Raval *et al.* proposed a 3D inductive power transfer system driven by a multiple phase power converter, based on a rotating magnetic field. This system created a cubic power zone which can charge the battery by loosely coupled magneto-motive force induction [14]–[16]. Zhang *et al.* proposed a WPT system for 3D, free-position and multi-object charging based on the properties of Helmholtz coils [17]. The downside of these 3D WPT systems is that the system's operation range is limited in the 'charging box'. To expand the charging range, E. S. Lee et al proposed a wide-range ubiquitous IPT system based on direct and quadrature (DQ) rotating magnetic-field. The transmitting (Tx) coils created high uniformity of magnetic field distribution and achieved 6-degrees of freedom charging of multiple receivers [18]. However, those characteristics of the system depend on the 3D structure of the receiving (Rx) coils as well. To increase the transmitted power and improve the transfer efficiency, Lim and Park proposed a novel WPT system based on a magnetic field beamforming technique with two crossed-loop transmitter coils [19]–[20]. By controlling the currents of two transmitter coils, the magnetic field can converge in a certain direction. However, this approach doesn't give a defined relationship between the magnetic field and the circuit. Seol and Chung derived the equivalent circuit model for a 2D WPT system [21], and D Lin et al provided the basic mathematical theory of omnidirectional wireless power transfer [22]. On the basis of the above techniques, Zhu *et al.* expanded the technique of magnetic field beamforming to higher dimensional WPT system and explicitly explained the relationship between the magnetic field and the circuit [23]. But those systems need the information of the receiver's position to realize the maximum power delivery. This control method is very useful to guide practical 3D WPT system design with more flexible coupling tolerance.

While expanding the charging range in 3D space around the system, all the previous works neglect the movements of the devices. In practice, mobile devices such as smartphone and watch, sorting and conveying robot probably need dynamic wireless charging in 3D space. Keeping dynamic maximum power transfer of the WPT system is the key point of current research.

This paper studies the maximum power transfer for the movable device based on an omnidirectional WPT system. The characteristic of the omnidirectional WPT system is analyzed first. Then, two different methods are theoretically analyzed and mathematically modeled according to the circuit model of the omnidirectional WPT system. By combining the input and output characteristics of the system and the characteristics of the proposed methods, the algorithms of each method achieve maximum power delivery without a communication link between the transmitter and the receiver. The validity of the two methods is verified in a prototype. And the different situations in which the two methods applied are discussed.

The rest of the paper is organized as follows: In section II, the modeling of the omnidirectional WPT system is derived. And the relationship between the input power and the load power is analyzed. In section III, the problem of maximum power delivery is analyzed without relying on communication between the transmitters and power receiver. And two methods for maximum power delivery are analyzed and mathematically modeled. In section IV, the real-time algorithms based on the analysis in section III are experimentally verified. And the difference between the two methods is discussed. In section V, a conclusion is drawn. The convergence of the algorithm for continuous operation is proved in the Appendix.

II. MODELING OF THE OMNIDIRECTIONAL WPT SYSTEM

A. STRUCTURE OF TWO CROSSED-LOOP WPT SYSTEM

The structure of the omnidirectional field orientation WPT system is shown in Fig. 1. The system has two transmitter coils, coil A and coil B, both of them are series connected with its own resonant capacitor. The transmitter coils are perpendicular to each other, which means the coupling factor between coil A and coil B is almost zero [19]. These transmitter coils are excited to generate omnidirectional magnetic field by two AC currents. Coil C is the receiver, connected with the resonant capacitor and the load. The energy is delivered by the magnetic coupling between the transmitter coils and the receiver coil. The cylindrical area is shown in Fig. 1 is the working range of this system, the receiver coil with load can receive energy everywhere around this cylindrical area at any pose.

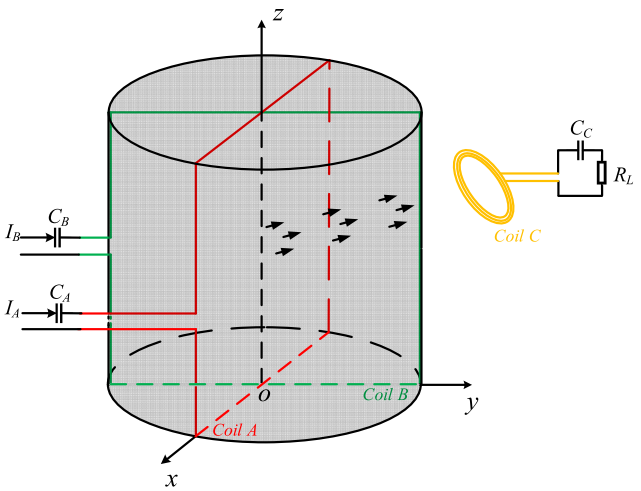

FIGURE 1. Space structure of the omnidirectional field orientation WPT system with two orthogonal transmitter coils.

B. CIRCUIT MODELLING OF TWO-DIMENSIONAL WPT SYSTEM

The magnetic coupling between the transmitters and the receiver can be described via a circuit model. The equivalent circuit model is shown in Fig. 2. U_{dc} and I_{dc} are the

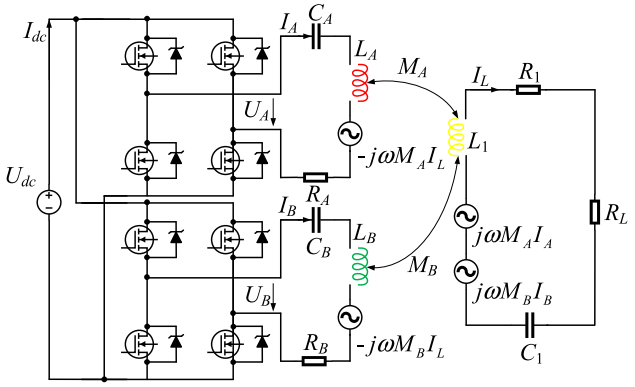

FIGURE 2. Equivalent model of the two crossed-loop coils wireless power transfer system.

DC voltage source and DC current of the system, respectively. I_A and I_B are two currents of transmitter coils, and I_L is the load current in the receiver coil. U_A and U_B are equivalent controlled voltage sources generated by two inverters, and they are used to adjust the current in the corresponding transmitter coil independently. L_A, L_B, and L_1 are the inductance of coil A, coil B, and the receiver coil, respectively. M_A and M_B are the mutual inductances between the transmitter coils and the receiver coil. R_A, R_B, and R_1 are the coil resistance of the transmitter coils and the receiver coil, respectively. C_A, C_B, and C_1 are the resonant capacitors of the transmitter coils and the receiver coil, respectively. The equivalent circuit model of the system can be described as:

$$U_A = I_A(R_A + jX_A) - j\omega M_A I_L \tag{1}$$
$$U_B = I_B(R_B + jX_B) - j\omega M_B I_L \tag{2}$$
$$0 = j\omega M_A I_A + j\omega M_B I_B - I_L(R_1 + R_L + j\omega X_1) \tag{3}$$

where

$$X_A = \omega L_A - 1/(\omega C_A), \quad X_B = \omega L_B - 1/(\omega C_B),$$
$$X_1 = \omega L_1 - 1/(\omega C_1)$$

To simplify the following calculation, the parameter of the transmitter coils and the resonant capacitor of the transmitter coils are considered as equal. $R = R_A = R_B$, $X = X_A = X_B$.

The current in transmitter coils are set as [22]:

$$\begin{bmatrix} I_A & I_B \end{bmatrix}^T = \mathbf{A}^T I \tag{4}$$

where

$$\mathbf{A} = [\sin\theta \quad \cos\theta], \quad \theta \in [0, 2\pi]$$

I is a positive real constant which is associated with the amplitude of the magnetic field. θ is regarded as the angle of the magnetic vector B, which is determined by the amplitude and phase difference of current I_A and I_B. According to equations (1-4), the load current can be calculated as follow.

$$I_L = \frac{j\omega I}{R_L + R_1 + jX_1}(M_A \sin\theta + M_B \cos\theta) \tag{5}$$

And its amplitude is:

$$\|I_L\| = \frac{\omega I\sqrt{M_A^2 + M_B^2}}{\sqrt{(R_L + R_1)^2 + X_1^2}}\left|\sin(\theta + \arctan\frac{M_B}{M_A})\right| \tag{6}$$

The active power of the load can be calculated as follow.

$$P_L = \frac{1}{2}\|I_L\|^2 R_L = \frac{\omega^2 I^2 R_L}{(R_L + R_1)^2 + X_1^2}(M_A \sin\theta + M_B \cos\theta)^2 \tag{7}$$

When the system is fixed, the active power of the load is determined by M_A, M_B, and θ. M_A and M_B are depended on the relative location of the transmitter coils and the receiver coil, and θ is determined by the current I_A and I_B. Therefore, the active power of the load can be expressed as follow.

$$P_L = K_L M^2 \tag{8}$$

where

$$K_L = \frac{\omega^2 I^2}{2(R_L + R_1)^2 + X_1^2}R_L, \quad M = (M_A \sin\theta + M_B \cos\theta)$$

K_L can be considered as a constant, and M is the unknown variable. In order to eliminate the communication from the transmitter part to the receiver part, the relationship between the load power and the input power of the system are discussed below.

The total consumed power of DC source P_{in} includes the power loss in the inverter P_{inv}, ohmic loss in the two transmitter coils P_{AB} and the power received by load coil P_{re}. The expression of P_{in} is shown as follow.

$$P_{in} = U_{dc} I_{dc} = P_{inv} + P_{AB} + P_{re} \tag{9}$$

And the power consumption of each part is calculated as follows.

$$P_{inv} = R_D I^2 + \frac{f_s}{T}\int_0^T \frac{1}{2} I U_{dc}(t_{off} + t_{on}) + \frac{1}{2} C_{oss} U_{dc}^2 dt \tag{10}$$

$$P_{AB} = I_A^2 R_A + I_B^2 R_B = I^2 R \tag{11}$$

$$P_{re} = P_L + \|I_1\|^2 R_1 = K_{re} M^2 \tag{12}$$

where

$$K_{re} = \frac{\omega^2 I^2}{2(R_L + R_1)^2 + X_1^2}(R_L + R_1)$$

The main power losses in the inverter including the conduction losses and switch losses. Conduction losses are depended on the conduction impedance R_D and the conduction current I. When I is set as a constant and R_D is fixed, the conduction losses can be considered as a constant. From the second part on the right side of equation (10), it can be known that switching loss are mainly depended on the operation frequency, DC voltage U_{dc}, conduction current I, the switch time $(t_{off} + t_{on})$ and the output capacitor of the switch C_{oss} [24], [25]. When the type of the switch and the operation frequency is determined, the switching loss is almost invariable.

In summary, the power loss in the inverter is constants when the value of I keeps unchanged.

Consider that the resistance of the transmission line is ignored, there is no other power dissipation in these coils except the equivalent coil resistance of them. From equation (11), the ohmic loss in transmitter coils also is constant during the operation of the system.

Similarly, in equation (12), K_{re} is fixed during the operation of the system. Hence, the power received by the load coil is directly proportional to the variable parameter M.

The efficiency of the system is described as:

$$\eta = \frac{P_L}{P_{in}} = \frac{P_L}{P_{inv} + P_{AB} + P_{re}} = \frac{K_L M^2}{C + K_{re} M^2} = \frac{K_L}{\frac{C}{M^2} + K_{re}} \tag{13}$$

where

$$C = P_{inv} + P_{AB}$$

C is the constant power dissipation during the operation of the system when I is fixed.

It can be known from equations (13), maximizing the variable parameter M will maximize the system efficiency. And the system input power P_{in} will be maximized simultaneously.

III. MATHEMATICAL MODELLING FOR MAXIMUM POWER DELIVERY

Section II presented the circuit model for the omnidirectional field orientation WPT system. In order to increase the transfer efficiency and reduce the charging time, maximum load active power delivery should be achieved when power pickup located at an arbitrary point in the space. The mathematical modeling of maximum power delivery can be generalized as an issue of the mathematical optimization problem.

$$\begin{cases} \underset{\theta}{\text{minmize}} & -P_L \\ \textit{subject to} & \theta \in [0, 2\pi) \end{cases} \tag{14}$$

From the analysis of power loss in Section II, it can be obtained that the P_L is directly proportional to P_{in}. P_L and P_{in} will be maximized at the same time. Therefore, the mathematical optimization problem above can be described as follows:

$$\begin{cases} \underset{\theta}{\text{minmize}} & -P_{in} \\ \textit{subject to} & \theta \in [0, 2\pi) \end{cases} \tag{15}$$

A. REALIZATION OF MAXIMUM POWER DELIVERY

1) METHOD I: PARAMETER IDENTIFICATION

Assume that the transmitter coils and the receiver coil are well-tuned, hence, X_A, X_B, and X_1 are all zero. The expression of the system input power can be rewritten as follows.

$$P_{in} = C + K \sin^2(\theta + \gamma) \tag{16}$$

where

$$K = \frac{1}{2} \frac{\omega^2 I^2}{R_L + R_1} (M_A^2 + M_B^2), \quad \gamma = \arctan \frac{M_B}{M_A}$$

In equation (16), C has been discussed in Section II. It's the constant power consumption of this system, which is related to the current I. The value of θ can be controlled by adjusting the current in transmitter coils I_A and I_B. K includes several unknown parameters, such as R_L, M_A and M_B. And γ contains two unknown parameters M_A and M_B. The value of M_A and M_B are determined by the position of the receiver coil. And every point in the working area of the system correspondingly has a determined value of M_A and M_B. That means the maximum value of P_{in} is only determined by the value of θ when the receiver enters the charging area. According to equation (16), when $\sin^2(\theta + \gamma) = 1$, $\mathbf{Max}(P_{in}) = C + K$, then $\theta_{\max} = \pi/2 - \gamma$ or $3\pi/2 - \gamma$. When $\sin^2(\theta + \gamma) = 0$, $\mathbf{Min}(P_{in}) = C$, then $\theta_{\min} = -\gamma$, or $\pi - \gamma$.

In order to identify these two unknown parameters (K and γ) in equation (16), at least two non-linear equations are required. Taking n different $\theta_1, \theta_2, \ldots, \theta_n$ as trial angles ($n > 2$), meanwhile, n different input power $P_{in1}, P_{in2}, \ldots, P_{inn}$ can be measured.

$$\begin{cases} P_{in1} = C + K \sin^2(\theta_1 + \gamma) \\ P_{in2} = C + K \sin^2(\theta_2 + \gamma) \\ \cdots \quad \cdots \\ P_{inn} = C + K \sin^2(\theta_n + \gamma) \end{cases} \tag{17}$$

From equation (17), any two of these equations can solve a set of K and γ, so C_n^2 sets of K and γ can be obtained, named K_i, γ_i (i is an integer, ranges from 1 to C_n^2).

$$\begin{cases} K^* = K_1, K_2, \ldots, K_{C_n^2} \\ \gamma^* = \gamma_1, \gamma_2, \ldots, \gamma_{C_n^2} \end{cases} \tag{18}$$

Assume that the expected values of K and γ are K^* and γ^*, because the noise of the measurement is Gaussian noise, hence K^* and γ^* can be calculated by the following equations.

$$\begin{cases} K^* = \dfrac{1}{C_n^2} \sum_{i=1}^{C_n^2} K_i \\ \gamma^* = \dfrac{1}{C_n^2} \sum_{i=1}^{C_n^2} \gamma_i \end{cases} \tag{19}$$

When K^* and γ^* are obtained, according to $\theta_{\max} = \pi/2 - \gamma^*$ or $3\pi/2 - \gamma^*$, the maximum power transfer can be realized by taking $\theta_{\max}$ as the optimal value.

$$P_{in\max} = C + K^* \sin^2(\theta_{\max} + \gamma^*)] \tag{20}$$

If the calculation speed of the digital processor is fast enough, this method can be used to figure out the optimal $\theta_{\max}$ soon after the system is started. However, this method only can be used to calculate $\theta_{\max}$ when M_A and M_B are fixed. That means this method needs a special trigger to restart the searching process if the receiver moves to another place.

2) METHOD II: GRADIENT DESCENT

In order to realize the real-time maximum power transfer, the algorithm of gradient descent is proposed. To find the optimal

value $\theta_{\max}$ and the maximum input power, the cost function of equation (16) is defined as follow.

$$f(\theta) = -P_{in} = -(C + K_{re}M^2) \tag{21}$$

When $f(\theta)$ minimized, the input power maximized. The minimum value of $f(\theta)$ is $-(C + K_{re}M_{\max}^2)$, where $M_{\max} = \sqrt{M_A^2 + M_B^2}$. For a dynamic receiver coil, the value of M_A and M_B keep changing all the time. And the gradient descent method is quite suited for this condition. The realization of dynamic maximum power transfer is shown as follows.

$$\frac{d\theta}{dt} = -\alpha \frac{df(\theta)}{d\theta} \tag{22}$$

α is the learning rate, which is an artificially defined positive number. Equation (22) also can be discretized as:

$$\theta(t+1) = \theta(t) - \alpha \frac{\partial f(\theta)}{d\theta} \Delta T \tag{23}$$

The derivative of $f(\theta)$ is calculated as follow.

$$\frac{\partial f(\theta)}{d\theta} = \frac{f(\theta + \Delta\theta) - f(\theta)}{\Delta\theta} \tag{24}$$

$\theta(t+1)$ is the angle of current control for next period, and $\theta(t)$ is the current angle for current control. And ΔT is the operation period of this system. $\partial f(\theta)/\partial\theta$ is used to calculate the gradient of $f(\theta)$. $\Delta\theta$ usually is set as a constant step size, which is sufficiently small. To speed convergence, an adaptive variable step size is adapted here. $\Delta\theta$ is calculated as follow.

$$\Delta\theta = \theta(t) - \theta(t-1) \tag{25}$$

The gradient descent method leads to the bottom of the bowl of the designed cost function, that is, to the point where the value of the cost function is minimal. In another word, the optimal value $\theta_{\max}$ and the maximum input power can be achieved by this method. Meanwhile, the convergence speed of the algorithm and the accuracy of the final result are affected by the value of α. The bigger the value of α is, the faster of the gradient descent converges, the greater of the fluctuation in the $\theta_{\max}$ and vice versa. Discretizing equations (22-25) by Euler's method, the procedure of gradient descent algorithm is shown in Table 1.

TABLE 1. Gradient descent algorithm.

Initialize $\theta(0)$ to zero and $\Delta\theta$ to 0.001;
$\theta \leftarrow \theta(0)$;
Set the reference value of *IA* and *IB* based on (4);
Execute current control unit the current is steady;
Compute $P_{in}(0)$ based on (9), $f(\theta) = P_{in}(0)$;
$\theta(t) \leftarrow \theta(0) + \Delta\theta$;
$\theta(t-1) = \theta(0)$;
While true:
$\theta \leftarrow \theta(t)$;
Set the reference value of *IA* and *IB* based on (4);
Execute current control unit the current is steady;
Compute $P_{in}(t)$ based on (9), then $f(\theta + \Delta\theta) = P_{in}(t)$;
Compute $\Delta\theta$ base on (24);
Compute $\partial f(\theta)/d\theta$ based on (23);
Compute $\theta(t+1)$ based on (22);
$f(\theta) = P_{in}(t)$, $\theta(t-1) = \theta(t)$, $\theta(t) = \theta(t+1)$;
End while.

IV. EXPERIMENTAL VERIFICATION OF THE PROPOSED ALGORITHM

A. OVERALL SYSTEM SETUP

Based on the previous theoretical analysis, an omnidirectional field orientation WPT system is implemented. Fig.3 shows the schematic block diagram of the 3D field orientation WPT system. The system's controller is composed of a floating-point digital signal processor

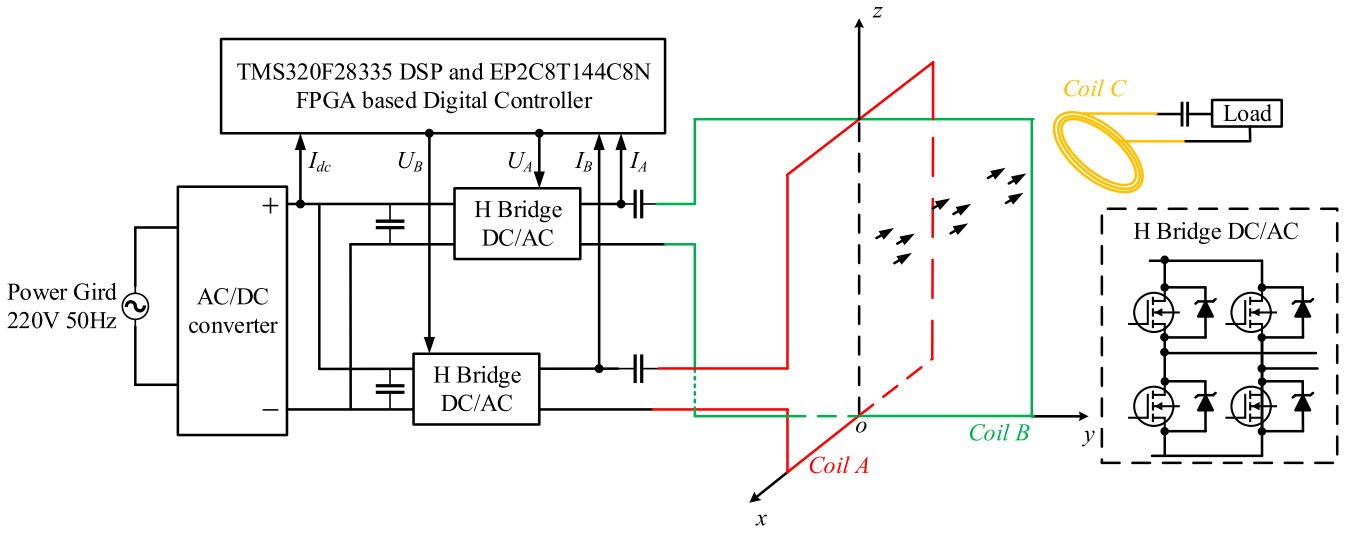

FIGURE 3. The schematic block diagram of the omnidirectional field orientation WPT system.

TABLE 2. Coil parameters of the two crossed-loop coils field orientation WPT system.

Transmit Coil	Frequency (kHz)	L (μH)	C (μF)	R (mΩ)	Length of side (mm)	Turns	Wire radius(mm)
Coil A	20	10.06	6.61	50.23	328	3	2.2
Coil B	20	10.09	6.59	50.30	328	3	2.2
Receiver Coil	Frequency (kHz)	L (μH)	C (μF)	R (mΩ)	Diameter (mm)	Turns	Wire radius(mm)
Coil C	20	245.51	0.2688	144.39	150	30	2.2

(DSP.TMS320F28335) and a field programmable gate array (FPGA.EP2C8J144C8N). DSP is in charge of mathematical calculation of the maximum power delivery algorithm and FPGA takes charge of generating driving signals for Metal-Oxide-Semiconductor Field-Effect Transistors (MOSFETs). AC/DC converter is connected with power grid and services as an ideal 12V DC voltage source. Two independent DC/AC converters are used to adjust the current in transmitter coils. Two square transmitter coils are designed to orthogonal to each other. And each coil has its own series resonant capacitor. The receiver coil connected with a series resonant capacitor and a resistance is used to simulate as the load. The inductance of each transmitter coil is designed as 10 μH, the inductance of receiver coil is designed as 245.51 μH, the capacitance of each series resonant capacitor for the transmitter is designed as 6.6 μF, the capacitance of a resonant capacitor for the receiver is designed as 0.2688 μF. The frequency of AC voltage generated by DC/AC converters is designed as 20 kHz. Each transmitter coil is a square with the length of side 328 mm and has three turns of Litz wire with radius 2.2 mm. The receiver coil (connected with load) is a circle whose diameter is 150mm and it has 30 turns of Litz wire. The actual coil parameter of the omnidirectional field orientation WPT system is shown in Table 2.

The experimental rig of the omnidirectional field orientation WPT system is shown in Fig. 4. The receiver coil's load is a resistance of 0.75 Ω. And the distance between the center of receiver coil and the center of two transmitter coils keeps constant. Transmitter coils current I_A and I_B are sampled by two independent current transducers HAS 50-S (LEM), which are used in current feedback control. The input DC current of the system I_{dc} is also sampled by another current transducer, which is used to calculate the input power of the system. The amplitude of I is set as 10 A. The experimental results of the implemented omnidirectional field orientation WPT system are presented below.

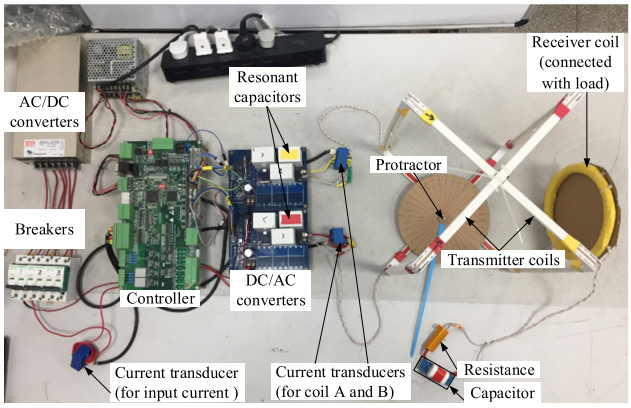

FIGURE 4. The prototype of the omnidirectional field orientation WPT system.

B. DYNAMIC EXPERIMENTS WITH MAXIMUM POWER TRANSFER

1) METHOD I: PARAMETER IDENTIFICATION

From the equations (17-20), it is clear that there is a trade-off relationship between the precision of the calculation result and the calculation time. In this experiment, the number of trial angles n is set as 4. The values of θ_1, θ_2, θ_3, θ_4 are set as 40°, 70°, 110° and 160°, respectively. Because the shaped magnetic field crossed the diagonal quadrant of the coordinate system, only the first and second quadrant are taken into consideration.

The process of the experiment is arranged as follow. First, turn on the system and complete the initialization. Then put the receiver coil at C1, which is shown in Fig. 5 (a), and keep its location unchanged until the current in transmitter coil is steady. Next, move the receiver from C1 to C2. The decrease of input power drives the controller restarted the current control function. Finally, the current I_A and I_B converged at another maximum power transfer point. The whole process of the experiment is shown in Fig. 5 (b).

Each time when the receiver coil changed its place in the working area, the trial angle traversed from θ_1 to θ_4. And four different input powers would be recorded. The controller calculated the maximum power point from (17-20) by using all the parameter obtained in the experiment, and the current control executed until the receiver coil moves again. In this experiment, the descent of the input power took the role of the trigger.

The waveforms from top to bottom in the following figures are the current in coil I_A, the current in coil B I_B, the induced voltage in receiver coil U_C and the current in receiver coil I_C, respectively.

The entire experiment consists of five parts which correspond to the region I to V shown in Fig. 5 (b). Region I represents the process of system initialization. In region II, the system traversed the pre-set values of θ_1, θ_2, θ_3 and θ_4. In region III, the maximum power point is found, and the

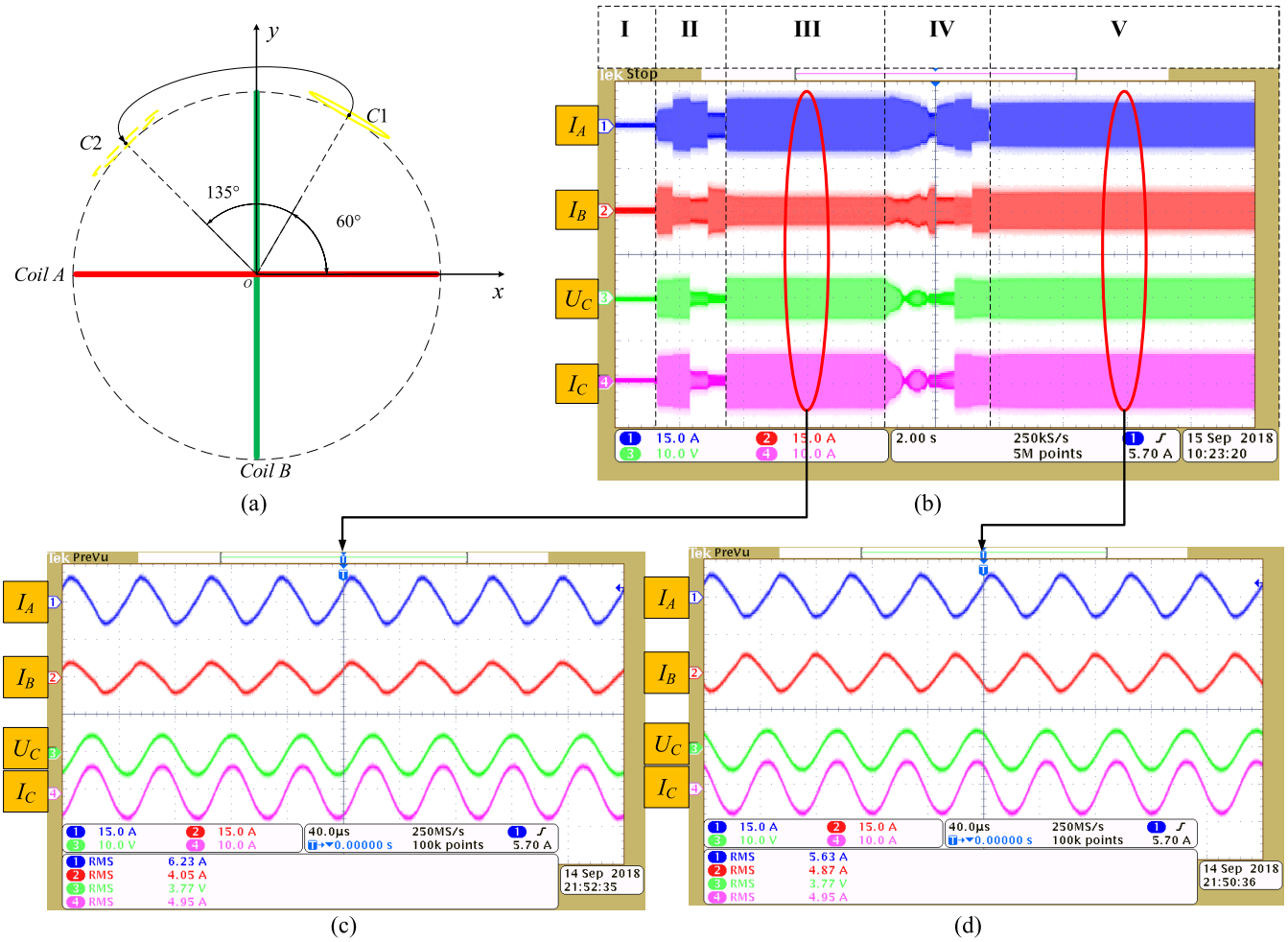

FIGURE 5. **The experimental waveforms of parameter identification method: (a) receiver coil moved from *C1* to *C2*; (b) Overall waveforms of parameter identification experiment; (c) Detailed waveforms in region III in Fig. 5(b); (d) Detailed waveforms in region V in Fig. 5(b).**

current in transmitter coils are controlled by the calculation result. At this time, $\theta_{max} \approx 60°$. The detailed waveforms of region III are shown in Fig. 5 (c). And the current in transmitter coils keeps constant in this part. The receiver coil moved to another place when the waveforms come to region IV. After the system triggered by the decline of input power, the controller started the procedure again. The procedure in this part is the same as that in region II. Finally, it came to region V, the shaped magnetic field pointed to the receiver which means the maximum power delivery is achieved again. At this time, $\theta_{max} \approx 135°$. The value of θ_{max} in Fig. 5 (c) and (d) can be proved by the amplitude of currents in transmitter coils.

Fig. 5(b) and (c) show detailed waveforms and the RMS of each waveform. The value of θ_{max} in the experiment is calculated by DSP, and it also can be verified by the RMS of currents in coil A and B. In Fig. 5 (b), the currents in coil A and coil B are 6.23 A and 4.05 A, respectively. Therefore, the calculated value of θ_{max} is 56.97°. In Fig. 5 (c), the current in coil A and coil B are 5.63 A and −4.87 A, respectively. ("−" means the opposite current direction.) The value of θ_{max} is calculated as 130.86°. Considering the error due to measurement and other factors, it can be confirmed that the parameter identification method is valid in maximum power delivery. And it is the feature of this method that the currents in transmitter coils keep constant after the value of θ_{max} has been figured out unless the receiver moves again. The transfer power to the load and the transfer efficiency shall be the highest if the receiver is absolutely still.

2) METHOD II: GRADIENT DESCENT

Unlike the parameter identification method, the gradient descent method could track the optimized θ dynamically. The only factor that affected the maximum power transfer is the magnitude of learning rate α. The learning rate α is set to 0.008 in this experiment. The experiment steps of gradient descent method are same as the previous experiment. First, turn on the system and complete the initialization. Then put the receiver coil at C1, which is shown in Fig. 6 (a), and keep its location unchanged until the current in transmitter coil is converged. Next, move the receiver from C1 to C2.

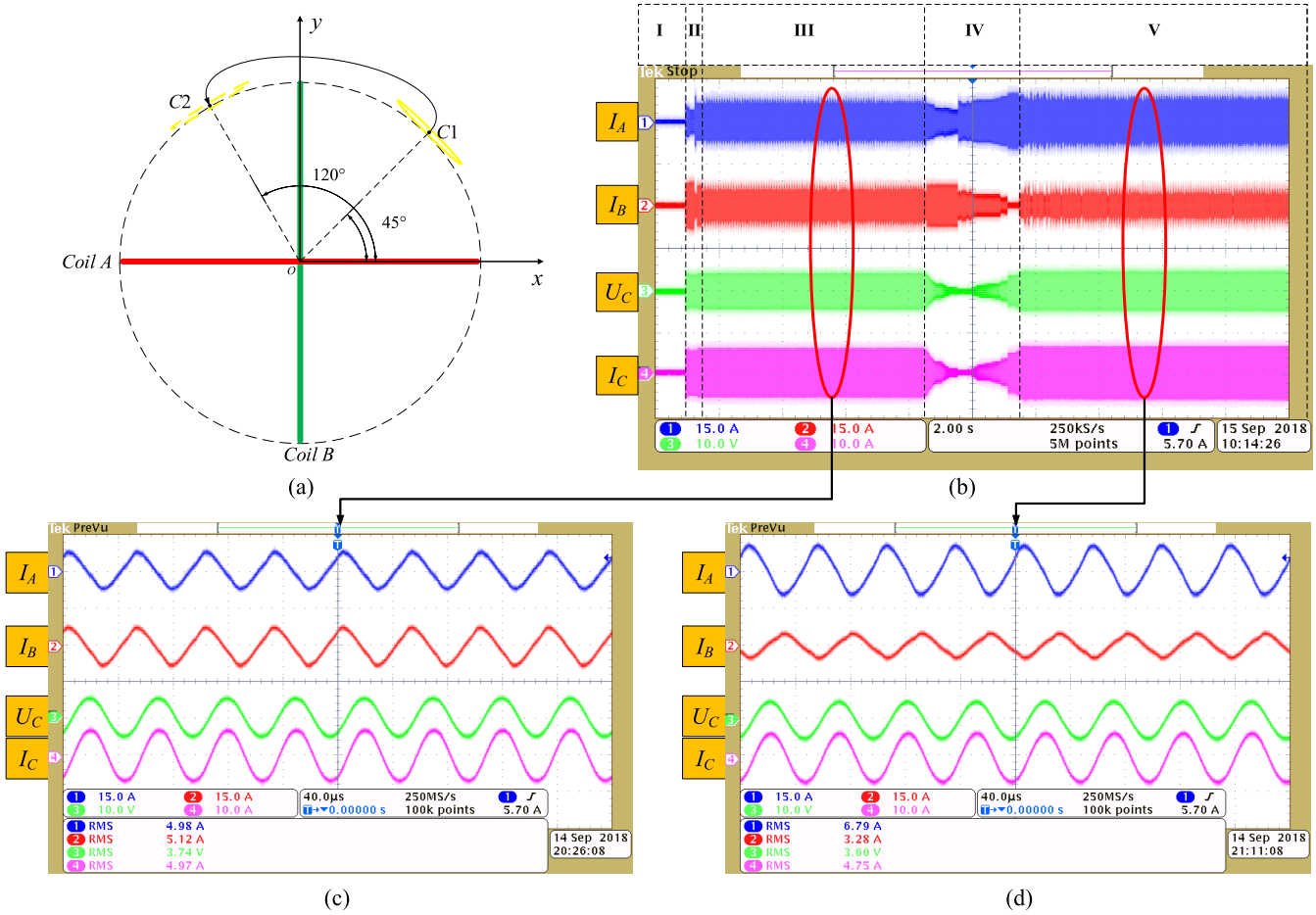

FIGURE 6. The experimental waveforms of gradient descent method: (a) receiver coil moved from *C1* to *C2*; (b) Overall waveforms of gradient descent experiment; (b) Detailed waveforms in region III in Fig. 6(b); (c) Detailed waveforms in region V in Fig. 6(b).

The gradient of $f(\theta)$ drove the change of current I_A and I_B, which made the input power maximize. Finally, the current I_A and I_B converged at another maximum power transfer point. The whole process of the experiment is shown in Fig. 6(b).

It's notable that the maximum power transfer is achieved dynamically. According to algorithm listed in Table 1, the minimal value of $f(\theta)$ is always tracked by the change of $\partial f(\theta)/\partial\theta$. And while the minimal value of $f(\theta)$ is achieved, the maximum power delivery is achieved simultaneously. The experiment process of gradient descent method is shown in Fig. 6 (a). The waveforms from top to bottom in the following figures are the current in coil I_A, the current in coil B I_B, the induced voltage in receiver coil U_C and the current in receiver coil I_C, respectively. Fig. 6 (b) the whole waveforms of the gradient descent experiment. In region I, the current in transmitter coils are changed by the gradient of $f(\theta)$, and the transmitted power Continuously increased. In region III, the maximum power transfer angle θ_{max} is found which is approximately equal to 45°. However, the currents in transmitter coils are oscillating in this part. The detailed waveforms of region III are shown in Fig. 6 (c). And the load power almost kept constant in this part. In region IV, the receiver coil moved from C1 to C2. The gradient of the input power changed at the same time. The value of θ_{max} gradually converged at the maximum power transfer point through the algorithm in Table 1. In region V, the load power reached its maximum value again. And at this time θ_{max} is approximately equal to 120°. Also, the current in transmitter coils is oscillating due to the inherent characteristics of the gradient descent. The detailed tracking result in region V is shown in Fig.6 (d).

The value of θ_{max} in the experiment is calculated by DSP, and it also can be calculated by the RMS of currents in coil A and B shown in Fig 6. In Fig. 6 (c), the currents in coil A and coil B are 4.98 A and 5.12 A, respectively. Therefore, the value of θ_{max} is calculated as 44.21°. In Fig. 6 (d), the current in coil A and coil B are 6.79 A and -3.28 A, respectively. The value of θ_{max} is calculated as 115.78°. In summary, the gradient descent method indeed transmitted the maximum power to the receiver coil in real-time. Even the receiver coil moves, the gradient of $f(\theta)$ drove the change of the current in transmitter coils to keep the maximum power transfer. Unlike the parameter identification method, the currents in transmitter coils won't be static. It is because that the gradient

descent method aims to minimize $f(\theta)$ which maximizes the input power simultaneously, and the Gaussian noise makes the measurement of the input power unstable. The calculated value of θ_{max} fluctuated up and down in the maximum power transfer point. And the current controlled by the calculated value of θ_{max} fluctuated in the same way. In addition, decreasing learning rate α can suppress the amplitude of the current fluctuations.

C. STEADY-STATE EXPERIMENTS

Considering both of the proposed methods can be used to achieve the maximum power transfer by focusing the magnetic field to the direction of the device. However, there is a different characteristic between them. In the parameter identification method, the currents in the transmitter coils are constant. While the currents fluctuated in the gradient descent method. To analyze the overall performance of the system working in different methods, the steady-state experiments are carried out.

The receiver coil is fixed at the point of $\theta = 45°$. In this case, the currents in transmitter coils are the same amplitude and phase when the maximum power transfer is achieved. First, the system runs under the no-load condition for a while. Then, let the system respectively run under the two methods. After the currents in transmitter coils are stabilized, let the system run for another 20 s. In both cases, the amplitude values of I are the same. The results of the steady-state experiments are shown in Fig. 7. The waveforms in Fig. 7 from the top to the bottom are the current in transmitter coils I_A, I_B and the DC current of the system, respectively. Consider that the performance of the voltage source is quite superior, U_{dc} is constant at 12 V during the experiment. Therefore, the system input power of each method can be directly obtained by the value of I_{dc}. In Fig. 7 (a), the mean value of I_{dc} is 0.915 A, which represents the loss power of the system under the no-load condition. Multiply I_{dc} by U_{dc}, the power loss of the system can be obtained which is 10.98W. Similarly, the input power of the system under different methods can be respectively calculated according to the mean value of I_{dc} in Fig. 7 (b) and (c). In Fig. 7 (b), the mean value of I_{dc} is 3.09 A, and it is 3.04 A in Fig. 7 (c). The calculated values of the system input power under the parameter identification method and the gradient descent method are 37.08W and 36.48W, respectively. And the efficiency of the two methods are calculated as 70.39% and 69.90%, respectively.

D. TRANSIENT EXPERIMENT

To test the dynamic response time of the proposed methods, a transient experiment in the extreme case is carried out. Before starting, the receiver coil is fixed at the point of $\theta = 45°$ and the magnetic field vector is set to be parallel to the receiver coil. First, let the system run for a while. And then, the operation mode changes to the proposed methods. During the whole experimental process, the waveforms of the currents in transmitter coils I_A, I_B, and the input current I_{dc} are recorded in Fig. 8.

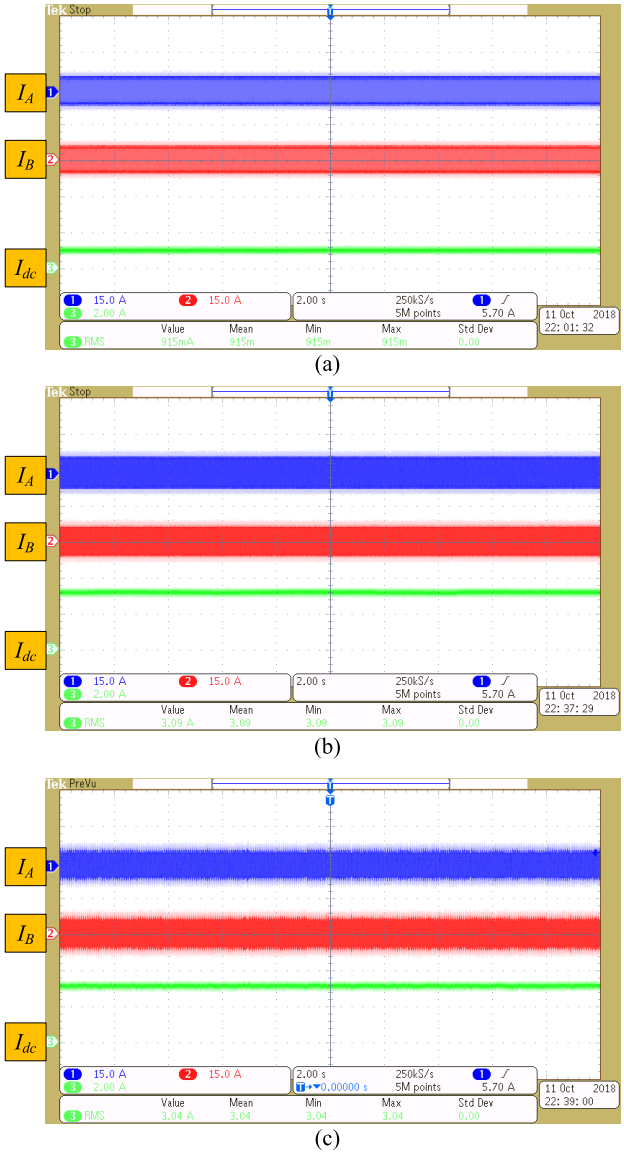

FIGURE 7. The results of the steady-state experiment: (a) the parameter identification method without load; (b) the parameter identification method with load; (c) the gradient descent method without load; (d) the gradient descent method with load.

Fig. 8 (a) shows the transient experimental result of the parameter identification method. In time interval t0, the system is working at the minimal power point, where the magnetic field vector is parallel to the receiver coil. In time interval t_1 and t_2, the system is running under the parameter identification method. In time interval t_1, the system is traversing the trial angles. The point of maximum power delivery will be calculated later, based on the power information collected in t_1. And in time interval t_2, the system worked at the maximum power transfer point. This method is somewhat similar to the traversal searching method. The final result is independent of the previous state of the system. As long as the receiver is stable at a certain position while the system traversing the pre-set trial angles, the target point of maximum power transfer can be precisely figured out.

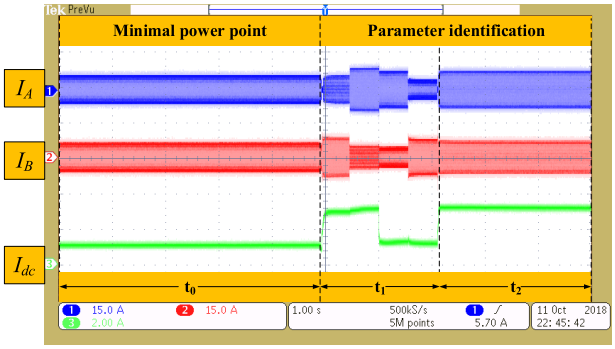

(a)

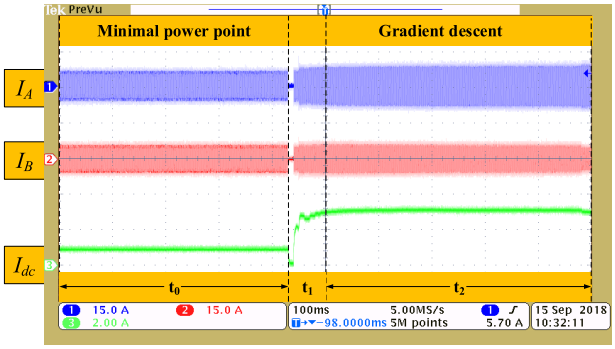

(b)

FIGURE 8. Experimental results for the dynamic response time of the proposed methods: (a) the parameter identification method; (b) the gradient descent method.

The transient experimental result of the gradient descent method is shown in Fig.8 (b). In time interval t_0, the system is working at the minimal power point. In time interval t_1 and t_2, the system is running under the algorithm of gradient descent. Thus, t_1 represents the dynamic response time. And in time interval t_2, the system worked at the maximum power transfer point. According to Fig. 8 (b), this method is a continuous operation method, whose dynamic response is related to the state if the previous cycle. And the dynamic response time in this experiment is less than 100ms. According to the mathematical proof of the convergence of the gradient descent method, this method can reach the maximum power transfer point regardless of the state of the system. Since this experiment is set at the extreme situation, it can be inferred that the dynamic response time of the gradient descent method is less than 100ms in general situations.

E. DISCUSSION ON PARAMETER IDENTIFICATION AND GRADIENT DESCENT METHODS

The two maximum power delivery methods in omnidirectional field orientation WPT system are verified by the above experimental results. For a practical wireless power transfer application, there are two main criteria to evaluate the proposed methods in this paper: speed and accuracy. The experimental results show that both the methods can be used to satisfy the above two points to a certain degree, and each method has its own practical application features.

The determining factors affecting the performance indicators of the parameter identification method are the number of trial angles n and the calculation speed of DSP. The greater of the number n, the greater of the accuracy of the calculation result, but also more time costs. In this experiment, the value of θ_{max} is calculated by DSP. It should be considered that n couldn't be too large as the calculation ability of the DSP is limited. Therefore, it's very important to select an appropriate number n when the accuracy of this method is limited by the calculation speed of the microprocessor and the interrupt period of the program.

In the experiment of gradient descent, the value of $\partial f(\theta)/\partial\theta$ is very large at the beginning. Therefore, the system will converge very quickly to the maximum power transfer point and $\partial f(\theta)/\partial\theta$ will be smaller and smaller at the same time. Eventually, the calculated value of θ_{max} will fluctuate up and down in the maximum power transfer point. During the operation process, the learning rate α has the greatest impact on the system performance indicators. The learning rate α is negatively correlated with accuracy, while it is positively correlated with the speed of convergence. It's worth mentioning that, gradient descent is a dynamic tracking process. The value of θ_{max} will fluctuate up and down in target point instead of stopping at a certain point.

In summary, the parameter identification method is applicable when the device is stationary most of the time. If the device moved to another position, the system can re-execute the parameter identification method to find the new maximum power transfer point. And it needs a more stable working environment. The accuracy of the final results depends on the precision of the system's parameters, and the deviation of the final result is caused by the disturbance when calculating the input power. Furthermore, once the final result is obtained, the magnetic field generated by the transmitter will also be fixed.

The gradient descent method can continuously achieve the maximum power transfer by following the gradient of $f(\theta)$. Hence, it is suitable for dynamic charging of frequently moving device. This method is able to adapt to different conditions by adjusting the magnitude of learning rate α and shows good performance in disturbance rejection and robustness. And the calculation process for the gradient descent method is quite simple. Therefore, this method could be applied in some cheaper microcontroller, which has lower calculating speed.

V. CONCLUSION

This paper studies the maximum power delivery methods for a movable device without a communication link between the transmitter and the receiver in an omnidirectional WPT system. The consistency of the variation of system input power and load power is analyzed and verified. The parameter identification method can find the maximum power transfer point when the receiver stops at an arbitrary position, according to the way of solving equations. And the gradient descent method can be used to track the maximum power

transfer point of a movable device in real-time by following the gradient change of the cost function. Different from the equation solving, the convergence of this continuous method is proofed based on LaSalle's invariance principle. Finally, the validity of the two methods is verified in a prototype. Both the methods can be used to achieve maximum power transfer for a movable load. And the output power and efficiency of the parameter identification method is 37.08W and 70.39%, while that of gradient descent method is 36.48Wand 69.90%. The gradient descent method has a fast dynamic response, while the parameter identification method can locate the device precisely. In practice, both methods can meet the needs of users in term of accuracy and speed by adjusting the number of the trial angle or the learning rate α.

APPENDIX

Proof of the convergence of the algorithm of gradient descent is demonstrated below.

Proof: It should be proved that every point starting in set D approaches to set M as $t \to \infty$, where

$$D = \{\theta \,|\theta \in [0, 2\pi)\}$$
$$M = \left\{\theta \in D \,|f(\theta) = -(C + K_{re}M_{\max}^2)\right\}$$

A Lyapunov function candidate $V(\theta)$ may be taken as

$$V(\theta) = \frac{-f(\theta) + C}{2K_{re}} \tag{26}$$

And it can be simplified as

$$V(\theta) = M^2 = (M_A \sin\theta + M_B \cos\theta)^2 \tag{27}$$

$V(\theta)$ can be thought of as a continuously differentiable function. The derivative of $V(\theta)$ is given by

$$\dot{V}(\theta) = \frac{dV}{d\theta}\frac{d\theta}{dt} \tag{28}$$

Substitute equations (22) and (27) into (28), the derivative of $V(\theta)$ is calculated as follow.

$$\dot{V}(\theta) = \frac{-\alpha}{K_{re}}(M_A \sin\theta + M_B \cos\theta)^2(M_A \cos\theta - M_B \sin\theta)^2 \tag{29}$$

Since α is a positive number, $\dot{V}(\theta)$ is negative semidefinite. It is obvious that D is a compact set that is positively invariant with respect to (26). Let E be the set of all points in D where $\dot{V}(\theta) = 0$. Let F be the largest invariant set in E. Then every point starting in D approaches F as $t \to \infty$ according to LaSalle's invariance principle [26]. The only thing needs to be proved is that $F \in M$. From equation (29), the sets of points in D where $\dot{V}(\theta) = 0$ can be expressed as

$$E_1 = \{\theta \in D | M_A \sin\theta + M_B \cos\theta = 0\}$$
$$E_2 = \{\theta \in D | M_A \cos\theta - M_B \sin\theta = 0\}$$

It is noticed that $E = E_1 \cup E_2$.

First, consider the set E_1. The value of θ in E_1 can be figured out as follow.

$$\theta = \arctan(-M_B/M_A) \tag{30}$$

Substituting (30) into (21), it can be obtained that $f(\theta) = -C$. Obviously, E_1 is out of M. Therefore, E_1 is not an invariant set.

Then, the value of θ in E_2 also can be figured out as follow.

$$\theta = \arctan(M_A/M_B) \tag{31}$$

Substituting (31) into (21), it can be obtained that $f(\theta) = -(C + K_{re}M_{\max}^2)$. It is easy to find that E_2 belongs to M. Therefore, E_2 is an invariant set and also the largest invariant set in the case when $\dot{V}(\theta) = 0$. So that $E_2 = F$, and it is obvious that $F \subset M$. Since every local optimal solution equals to each other, all of them are the global optimal solution. The analytic proof is derived.

REFERENCES

[1] A. Chandrasekhar, N. R. Alluri, M. S. P. Sudhakaran, Y. S. Mok, and S.-J. Kim, "A smart mobile pouch as a biomechanical energy harvester towards self-powered smart wireless power transfer applications," *Nanoscale*, vol. 9, no. 28, pp. 9818–9824, Jul. 2017, doi: 10.1039/c7nr00110j.

[2] A. P. Hu and S. Hussmann, "Improved power flow control for contactless moving sensor applications," *IEEE Power Electron Lett.*, vol. 2, no. 4, pp. 135–138, Dec. 2004, doi: 10.1109/LPEL.2004.841311.

[3] P. Si, A. P. Hu, S. Malpas, and D. Budgett, "A frequency control method for regulating wireless power to implantable devices," *IEEE Trans. Biomed. Circuits Syst.*, vol. 2, no. 1, pp. 22–29, Mar. 2008, doi: 10.1109/TBCAS.2008.918284.

[4] L. Li, H. Liu, H. Zhang, and W. Xue, "Efficient wireless power transfer system integrating with metasurface for biological applications," *IEEE Trans. Ind. Electron.*, vol. 65, no. 4, pp. 3230–3239, Apr. 2018, doi: 10.1109/TIE.2017.2756580.

[5] H. A. Fadhil, S. G. Abdulqader, and S. A. Aljunid, "Implementation of wireless power transfer system for Smart Home applications," in *Proc. IEEE 8th GCC Conf. Exhib.*, Muscat, Oman, Feb. 2015, pp. 1–4, doi: 10.1109/IEEEGCC.2015.7060042.

[6] M. Sugino and T. Masamura, "The wireless power transfer systems using the class E push-pull inverter for industrial robots," in *Proc. IEEE Wireless Power Transf. Conf. (WPTC)*, Taipei, Taiwan, May 2017, pp. 1–3, doi: 10.1109/WPT.2017.7953901.

[7] S. Li and C. C. Mi, "Wireless power transfer for electric vehicle applications," *IEEE J. Emerg. Sel. Topics Power Electron.*, vol. 3, no. 1, pp. 4–17, Mar. 2014, doi: 10.1109/jestpe.2014.2319453.

[8] F. Lu, H. Zhang, and C. Mi, "A two-plate capacitive wireless power transfer system for electric vehicle charging applications," *IEEE Trans. Power Electron.*, vol. 33, no. 2, pp. 964–969, Feb. 2018, doi: 10.1109/TPEL.2017.2735365.

[9] F. Lu, H. Zhang, H. Hofmann, and C. C. Mi, "An inductive and capacitive combined wireless power transfer system withLC-compensated topology," *IEEE Trans. Power Electron.*, vol. 31, no. 12, pp. 8471–8482, Dec. 2016, doi: 10.1109/TPEL.2016.2519903.

[10] R. Mai, Y. Liu, Y. Li, P. Yue, G. Cao, and Z. He, "An active-rectifier-based maximum efficiency tracking method using an additional measurement coil for wireless power transfer," *IEEE Trans. Power Electron.*, vol. 33, no. 1, pp. 716–728, Jan. 2018, doi: 10.1109/TPEL.2017.2665040.

[11] K.-S. Yoon, S.-H. Lee, I.-K. Cho, H.-J. Lee, and G.-H. Cho, "Dual receiver coils wireless power transfer system with interleaving switching," *IEEE Trans. Power Electron.*, vol. 33, no. 12, pp. 10016–10020, Dec. 2018, doi: 10.1109/TPEL.2018.2824019.

[12] L. Zhao, D. J. Thrimawithana, and U. K. Madawala, "Hybrid bidirectional wireless EV charging system tolerant to pad misalignment," *IEEE Trans. Ind. Electron.*, vol. 64, no. 9, pp. 7079–7086, Sep. 2017, doi: 10.1109/TIE.2017.2686301.

[13] L. Zhao, D. J. Thrimawithana, U. K. Madawala, P. Hu, and C. C. Mi, "A misalignment tolerant series-hybrid wireless EV charging system with integrated magnetics," *IEEE Trans. Power Electron.*, to be published, doi: 10.1109/TPEL.2018.2828841.

[14] P. Raval, D. Kacprzak, and A. P. Hu "3D inductive power transfer power system," *Wireless Power Transf.*, vol. 1, no. 1, pp. 51–64, Apr. 2014, doi: 10.1017/wpt.2014.7.

[15] P. Raval, D. Kacprzak, and A. P. Hu, "Multiphase inductive power transfer box based on a rotating magnetic field," *IEEE Trans. Ind. Electron.*, vol. 62, no. 2, pp. 795–802, Feb. 2015, doi: 10.1109/TIE.2014.2334666.
[16] P. Raval, D. Kacprzak, and A. P. Hu, "Analysis of flux leakage of a 3-D inductive power transfer system," *IEEE J. Emerg. Sel. Topics Power Electron.*, vol. 3, no. 1, pp. 205–214, Mar. 2015, doi: 10.1109/JESTPE.2014.2310192.
[17] W. Zhang *et al.*, "High-efficiency wireless power transfer system for 3D, unstationary free-positioning and multi-object charging," *IET Electr. Power Appl.*, vol. 12, no. 5, pp. 658–665, Apr. 2018, doi: 10.1049/iet-epa.2017.0581.
[18] E. S. Lee, J. S. Choi, H. S. Son, S. H. Han, and C. T. Rim, "Six degrees of freedom wide-range ubiquitous IPT for IoT by DQ magnetic field," *IEEE Trans. Power Electron.*, vol. 32, no. 11, pp. 8258–8276, Nov. 2017, doi: 10.1109/TPEL.2017.2691063.
[19] Y. Lim, H.-S. Ahn, and J. Park, "Analysis of antenna structure for energy beamforming in wireless power transfer," *IEEE Trans. Antennas Propag.*, vol. 65, no. 11, pp. 6085–6094, Nov. 2017, doi: 10.1109/TAP.2017.2754326.
[20] Y. Lim and J. Park, "A novel phase-control-based energy beamforming techniques in nonradiative wireless power transfer," *IEEE Trans. Power Electron.*, vol. 30, no. 11, pp. 6274–6287, Nov. 2015, doi: 10.1109/TPEL.2014.2379672.
[21] W.-K. Seol and S.-K. Chung, "Current vector control of wireless power transfer system with 2D transmitting coils," *Electron. Lett.*, vol. 54, no. 2, pp. 91–93, Jan. 2018, doi: 10.10149/el.2017.3816.
[22] D. Lin, C. Zhang, and S. Y. R. Hui, "Mathematical analysis of omnidirectional wireless power transfer—Part-I: Two-dimensional systems," *IEEE Trans. Power Electron.*, vol. 32, no. 1, pp. 625–633, Jan. 2017, doi: 10.1109/TPEL.2016.2523500.
[23] Q. Zhu, M. Su, Y. Sun, W. Tang, and A. P. Hu, "Field orientation based on current amplitude and phase angle control for wireless power transfer," *IEEE Trans. Ind. Electron.*, vol. 65, no. 6, pp. 4758–4770, Jun. 2018, doi: 10.1109/TIE.2017.2767556.
[24] T. Nussbaumer, M. Baumann, and J. W. Kolar, "Comprehensive design of a three-phase three-switch buck-type PWM rectifier," *IEEE Trans. Power Electron.*, vol. 22, no. 2, pp. 551–562, Mar. 2007, doi: 10.1109/TPEL.2006.889987.
[25] Y. Xiong, S. Sun, H. Jia, P. Shea, and Z. J. Shen, "New physical insights on power MOSFET switching losses," *IEEE Trans. Power Electron.*, vol. 24, no. 2, pp. 525–531, Feb. 2009, doi: 10.1109/TPEL.2008.2006567.
[26] H. K. Khalil, *Nonlinear Systems*, 3rd ed. Lansing, MI, USA: Publishing House of Electronics Industry, 2002, pp. 128–133.

MEI SU was born in Hanshou, Hunan, China, in 1967. She received the B.S. degree in automation and the M.S. and Ph.D. degrees in electric engineering from the School of Information Science and Engineering, Central South University, in 1989, 1992, and 2005, respectively. Since 2006, she has been a Professor with the School of Information Science and Engineering, Central South University. Her research interests include matrix converter, adjustable speed drives, and wind energy conversion system.

ZIXI LIU was born in Chenzhou, Hunan, China, in 1993. He received the B.S. degree in electrical engineering and automation from Sichuan University, Chengdu, China, in 2016. He is currently pursuing the M.S. degree in electrical engineering. His research interests include wireless power transfer.

QI ZHU was born in Tongling, Anhui, China, in 1993. He received the B.S. degree in electrical engineering and automation from Central South University, Changsha, China, in 2014, where he is currently pursuing the Ph.D. degree in electrical engineering. Since 2017, he has been a joint Ph.D. student founded by the China Scholarship Council at the University of Auckland, Auckland, New Zealand. His research interests include wireless power transfer and matrix converter.

AIGUO PATRICK HU was born in Yanchuan, Shanxi, China. He received the B.E. and M.E. degrees from Xi'an Jiaotong University, Xi'an, China, in 1985 and 1988, respectively, and the Ph.D. degree from the University of Auckland, Auckland, New Zealand, in 2001. He was a Lecturer, the Director of the China Italy Cooperative Technical Training Center, Xian, and the General Manager of a technical development company. Funded by Asian2000 Foundation, he was with the National University of Singapore for a semester as an exchange Post-Doctoral Research Fellow. He is currently with the Department of Electrical and Computer Engineering, University of Auckland, and also the Head of Research of PowerbyProxi, Ltd. He holds 15 patents in wireless/contactless power transfer and microcomputer control technologies, published more than 200 peer-reviewed journal and conference papers, authored a monograph on wireless inductive power transfer technology, and contributed four book chapters.